Analytica Chimica Acta 1065 (2019) 12–20

Contents lists available at ScienceDirect

Analytica Chimica Acta

journal homepage: www.elsevier.com/locate/aca

New bioanalytical platform based on the use of avidin for the successful exfoliation of multi-walled carbon nanotubes and the robust anchoring of biomolecules. Application for hydrogen peroxide biosensing

F.A. Gutierrez, M.D. Rubianes**, G.A. Rivas*

INFIQC, Facultad de Ciencias Químicas, Universidad Nacional de Córdoba, Haya de la Torre S/N, Ciudad Universitaria, 5000, Córdoba, Argentina

HIGHLIGHTS

- Avidin successfully disperses MWCNTs and provides them of bio-recognition properties.
- Avidin maintains their recognition properties even after the drastic dispersing conditions.
- GCE/MWCNTs-avidin is a versatile platform to immobilize biotynilated residues.
- Biotinylated HRP was attached to GCE/MWCNTs-avidin as proof-of-concept.
- GCE/MWCNT-avidin/b-HRP allowed the highly sensitive quantification of H_2O_2.
- GCE/MWCNT-avidin/b-HRP was successfully used for detecting of H_2O_2 in real samples.

GRAPHICAL ABSTRACT

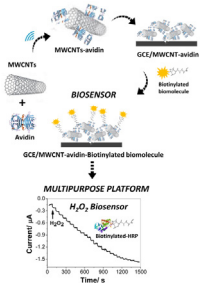

ARTICLE INFO

Article history:
Received 29 December 2018
Received in revised form
5 March 2019
Accepted 11 March 2019
Available online 22 March 2019

Keywords:
Carbon nanotubes functionalization
Multi-walled carbon nanotubes
Avidin
Horseradish peroxidase
Hydrogen peroxide biosensor

ABSTRACT

We are reporting an innovative building-block for the development of biosensors based on the non-covalent functionalization of multi-walled carbon nanotubes (MWCNTs) with avidin (MWCNTs-avidin). In this work, at variance with previous reports, avidin has the double role of simultaneously being the exfoliating agent of MWCNTs and the platform for anchoring different biotinylated biomolecules. The optimum dispersion was obtained by sonicating for 5.0 min 0.50 mgmL^{-1} MWCNTs with 1.00 mgmL^{-1} avidin solution prepared in 50:50 v/v ethanol/water. As proof-of-concept, we immobilized biotinylated horseradish peroxidase (b-HRP) at glassy carbon electrodes (GCE) modified with MWCNTs-avidin to develop a hydrogen peroxide biosensor using hydroquinone as redox mediator. Surface plasmon resonance, electrochemical impedance spectroscopy, cyclic voltammetry and amperometry demonstrated that, even after the partial denaturation of avidin due to the drastic conditions used to functionalize the MWCNTs, it preserves the biorecognition properties and efficiently interacts with biotinylated horseradish peroxidase (b-HRP). The analytical characteristics of the resulting hydrogen peroxide biosensor are the following: linear range between 1.0×10^{-6} M and 1.4×10^{-5} M, sensitivity of (1.37 ± 0.04) x 10^5

* Corresponding author.
** Corresponding author.
E-mail addresses: rubianes@fcq.unc.edu.ar (M.D. Rubianes), grivas@fcq.unc.edu.ar (G.A. Rivas).

https://doi.org/10.1016/j.aca.2019.03.022

μAM^{-1}, detection limit of 24 nM and reproducibility of 2.9%. The sensor was challenged with different samples, a mouthwash solution, human blood serum and milk, with very good performance.

1. Introduction

The exceptional properties of carbon nanostructures have made them very attractive materials for the construction of electrochemical (bio)sensors [1–3]. Particularly, carbon nanotubes (CNTs) have been widely used due to their unique electronic, structural, mechanical and catalytic properties, their capacity to interact with different biomolecules, and their multiple possibilities of functionalization [4–6].

Due to the important interactions between tubes through van der Waals forces and π-π stacking, CNTs requires some functionalization to minimize their aggregation and to allow them to participate in the construction of electrochemical (bio)sensors [7,8]. The non-covalent scheme has received enormous attention since it makes possible an efficient functionalization of CNTs without disturbing their electronic characteristics. Supramolecular complexes were obtained after the interaction of CNTs with different polymers [9]. For instance, chitosan [10], polyethylenimine [11,12], Nafion [13], poly(4-vinylpyridine) [14], poly(lysine) [15], poly(arginine) [16], poly(histidine) [17], and poly(aniline) [18] have been successfully used for the preparation of CNTs-based electrochemical biosensors.

We have proposed an interesting and original strategy to develop CNTs-based electrochemical sensors by direct functionalization of multiwall carbon nanotubes (MWCNTs) with different biomolecules. The main challenge of this strategy was to obtain supramolecular architectures where the biomolecules maintain as much as possible their biocatalytic/bioaffinity properties and allow to obtain sensitive and well-defined analytical signals that ensuring a competitive biosensing. In fact, we have reported the use of glucose oxidase (GOx) [19] cytochrome c [20,21] and calf-thymus double stranded DNA (dsDNA) [22,23] to non-covalently functionalize MWCNTs. In general, the functionalization was performed by ultrasonicating the mixture of the biomolecule (prepared in a 50/50 v/v ethanol/water solution) and MWCNTs for a given time. As a consequence of these drastic conditions to prepare the dispersions, the biomolecules that supported the carbon nanostructures suffered a partial denaturation. However, even after this partial denaturation, the enzymes recognized their substrates (glucose in the case of GOx and hydrogen peroxide in the case of cytochrome c) and dsDNA recognized the know intercalator promethazine. Therefore, it was possible to obtain successful glucose, hydrogen peroxide and promethazine electrochemical biosensors once the resulting dispersions were immobilized at glassy carbon electrodes (GCE).

In this work, we report an innovative building-block for the development of biosensors based on the use of avidin in two directions, to exfoliate multi-walled carbon nanotubes (MWCNTs) (MWCNTs-avidin) and to work as platform to immobilize a given biotinylated molecule to obtain the desired biosensor. In this work, we selected a biotinylated horseradish peroxidase (b-HRP) as proof-of-concept of the interaction between the avidin that supports the MWCNTs and a biotinylated biomolecule. In the following sections, we present the characterization of GCE modified with avidin-functionalized MWCNTs (GCE/MWCNTs-avidin), the evaluation of the biorecognition properties of GCE/MWCNTs-avidin in the presence of b-HRP, and the analytical performance of the resulting GCE/MWCNTs-avidin/b-HRP for the highly sensitive hydrogen peroxide biosensing using hydroquinone as redox mediator.

2. Experimental section

2.1. Chemicals

Hydrogen peroxide (30% v/v aqueous solution) was purchased from Baker. Avidin of egg white (Ref: 434401) and biotinylated horseradish peroxidase (b-HRP, Ref: 432040) were obtained from Life Technology-Invitrogen (USA). Hydroquinone (HQ) and benzoquinone were received from Sigma-Aldrich. Multiwalled carbon nanotubes powder (MWCNTs, diameter (30 ± 15) nm, length 1–5 μm) was purchased from NanoLab, U.S.A.). Other chemicals were reagent grade and used without further purification. Ultrapure water (ρ = 18 MΩcm) from a Millipore-MilliQ system was used for preparing all the solutions. A 0.100 M saline phosphate buffer solution (PBS) pH 7.40 was used as supporting electrolyte and (GCE/MWCNTs-avidin)/(b-HRP) interaction buffer. PBS solution with 0.010% Tween-20 was used as washing buffer after interaction of GCE/MWCNTs-avidin with b-HRP or HRP to remove the unspecific bond protein.

2.2. Apparatus

Electrochemical experiments were carried out with TEQ 4 and Autolab PGSTAT128 N potentiostats. A platinum wire and Ag/AgCl, 3M NaCl (BAS, Model RE-5B) were used as auxiliary and reference electrodes, respectively. All potentials are referred to the latter. A magnetic stirrer (BASi Cell stand) set at 800 rpm and a stirring bar provided the convective transport during the amperometric measurements.

Scanning Electron Microscopy (SEM) images were obtained with a Field Emission Gun Scanning Electron Microscope (Zeiss, ΣIGMA model). The samples were prepared by depositing the dispersion of MWCNTs-avidin at glassy carbon disks and drying at room temperature. UV-Vis experiments were performed with a Shimadzu UV 1700 Pharma spectrometer. Circular dichroism spectra were recorded with a JASCO Model J-810 spectropolarimeter. FT-IR spectra were obtained with a Nicolet 5-SX C spectrometer.

Sonication treatments were carried out with a sonicator probe VCX 130W (Sonics & Materials, Inc.) of 20 kHz frequency with a titanium alloy microtip (3 mm diameter).

Amperometric experiments were performed at −0.100 V in the supporting electrolyte solution by successive additions of hydrogen peroxide. Electrochemical impedance spectroscopy (EIS) experiments were carried out in the supporting electrolyte solution by applying a sinusoidal potential perturbation of 10 mV in the frequency range of 10^5–10^{-1} Hz. The working potential was the formal potential of a 2.0×10^{-3} M hydroquinone/benzoquinone solution (0.050 V). The impedance spectra were analyzed and fitted using the Z-view program.

Electrochemical capacitance spectroscopy (ECS) is based on impedimetric measurements by converting the complex impedance, Z*(w) into a complex capacitance, C*(w). The spectra were

obtained in the supporting electrolyte solution for frequencies ranging from 1 MHz to 0.1 Hz with an amplitude of 10 mV (peak to peak) at a stationary potential of 0.0 V.

SPR measurements were performed with a single chanel AUTOLAB SPRINGLE instrument (Eco Chemie), using Au disks (BK7). Sample solutions (60 μL) were injected manually into the cuvette. The measurements were carried out under stationary conditions at (25 ± 1) °C. The analytical signal was the change in the plasmon resonance angle ($\Delta\theta_{SPR}$) for Au/MWCNT-avidin obtained as the difference between θ_{SPR} after and before the addition of b-HRP (once the surfaces were washed with the washing buffer).

2.3. Preparation of the dispersions

a) The dispersion of MWCNTs with avidin (MWCNTs-avidin) was obtained by mixing 0.50 mg of MWCNTs with 1.00 mL of avidin solution (1.00 mgmL^{-1} prepared in 50:50 v/v ethanol/water) followed by sonication for 5.0 min with ultrasonic probe.

(b) The dispersion of MWCNTs in 50/50 v/v ethanol/water was obtained by mixing 1.00 mg of MWCNTs with 1.00 mL of 50:50 v/v ethanol/water followed by sonication for 5.0 min with ultrasonic probe.

2.4. Preparation of GCE modified with the dispersions

Before modification, GCE was polished with alumina slurries of 1.0, 0.30, and 0.05 μm for 2 min each. After that, the GCEs were modified by dropping 20 μL of MWCNT-avidin dispersion on the top of the surfaces followed by the evaporation of the solvent at room temperature (GCE/MWCNTs-avidin). Similar protocol was followed to prepare GCE modified with MWCNTs dispersed in 50/50 v/v ethanol/water (GCE/MWCNTs) using the corresponding dispersion.

2.5. Preparation of GCE/MWCNT-avidin modified with biotinylated horseradish peroxidase

GCE/MWCNTs-avidin was modified with b-HRP (GCE/MWCNTs-avidin/b-HRP) by dipping the electrode in a b-HRP solution (1.00 mgmL^{-1} prepared in 0.100 M PBS pH 7.40) for 30 min at room temperature. Similar protocol was used for preparing the GCE/MWCNT-avidin modified with non-biotinylated HRP (GCE/MWCNT-avidin/HRP).

3. Results and discussion

3.1. Characterization of GCE modified with MWCNT-avidin. Effect of avidin concentration

Fig. 1A displays cyclic voltammograms for 1.0×10^{-3} M hydroquinone at GCE/MWCNT (a) and GCE/MWCNT-avidin (b). At GCE/MWCNTs the potentiodynamic profile shows the typical quasi-reversible electrooxidation of hydroquinone, with a cathodic peak current ($i_{p,c}$) of 289 μA and an anodic peak current ($i_{p,a}$) of 287 μA. At variance with this behavior, at GCE/MWCNTs-avidin, there is an important decrease of the reduction and oxidation peak currents ($i_{p,c} = 88$ μA; $i_{p,a} = 96$ μA). Since hydroquinone has to be adsorbed at sp^2 carbon to allow the electron transfer [24], it is a good indicator of the electrode-surface state. Therefore, these results indicate that the avidin that supports the CNTs produces a blockage of the electrode surface.

Fig. 1B depicts Nyquist plots obtained at 0.050 V for GCE/MWCNTs (a) and GCE/MWCNTs-avidin (b) using 2.0×10^{-3} M hydroquinone/benzoquinone as redox markers. The experimental data (symbols) were fitted with a Randles circuit (solid line) where R_s is the electrolytic resistance, R_{ct} the charge transfer resistance, C_{dl} the double layer capacitance, and W the Warburg impedance. The increment in the semicircle portion observed at higher frequencies for GCE/MWCNT-avidin, is a clear indication of the increase of R_{ct} due to the blocking effect of the protein that supports the MWCNTs ((3.0 ± 0.2) x 10^3 Ω and (1.10 ± 0.09) x 10^3 Ω, for GCE/MWCNT-avidin and GCE/MWCNTs, respectively), in agreement with the results shown in Fig. 1A.

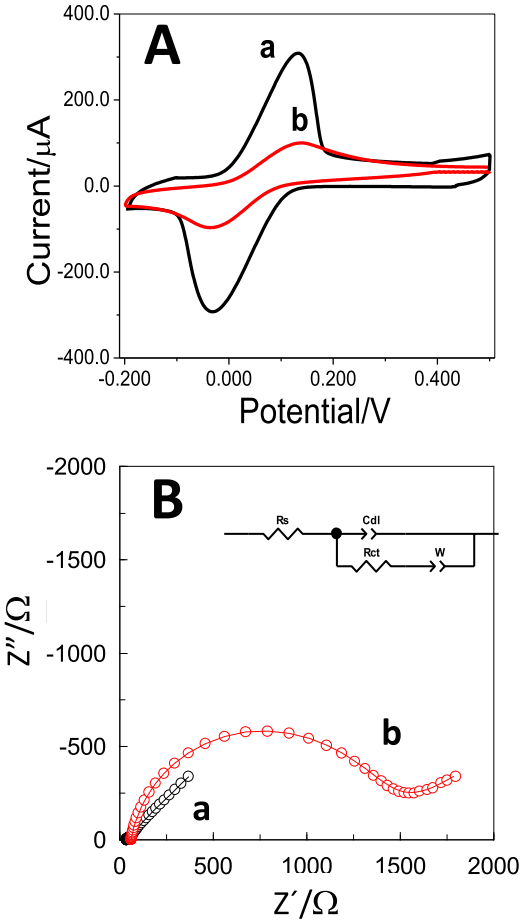

Fig. 1. A) Cyclic voltamograms for 1.0×10^{-3} M hydroquinone obtained at GCE/MWCNT (a) and GCE/MWCNT-avidin (b). Scan rate: 0.100 Vs^{-1}. B) Nyquist plots for 2.0×10^{-3} M hydroquinone/benzoquinone obtained at GCE/MWCNT (a) and GCE/MWCNT-avidin (b). Frequency range: 10 KHz to 10 mHz; Potential perturbation: 10 mV; Working potential: 0.050 V. Inset: Randles circuit. Supporting electrolyte: 0.100 M PBS pH 7.40.

Taking into account that the dispersing agent/CNTs ratio has demonstrated to be a critical aspect to obtain an efficient functionalization of carbon nanostructures [25] we evaluated the effect of the avidin concentration used to prepare the dispersions on the performance of GCEs modified with the resulting dispersions. Fig. 2A depicts the variation of the peak-potential separation (ΔE_p) for 1.0×10^{-3} M hydroquinone obtained from cyclic voltammograms performed at GCE modified with MWCNTs (0.50 mgmL^{-1}) dispersed with avidin solutions of different concentrations (from 0.25 to 2.00 mgmL^{-1}). ΔE_p increases with the increment of avidin concentration in the dispersions up to 1.0 mgmL^{-1}, demonstrating the influence of the amount of avidin present in the dispersion on the charge transfer of the redox probe. ΔE_p values are summarized in Table SI-1.

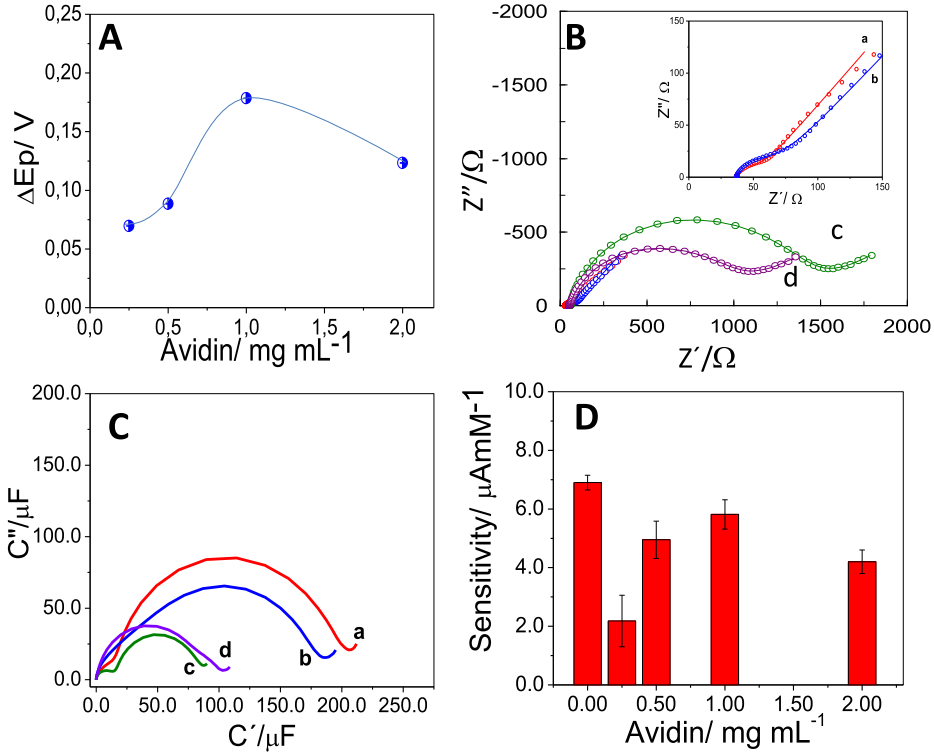

Fig. 2. A) Peak potential separation (ΔEp) for 1.0×10^{-3} M hydroquinone as a function of the concentration of avidin used to disperse the MWCNTs (from 0.25 to 2.00 $mgmL^{-1}$) obtained from cyclic voltammograms. Scan rate: 0.100 Vs^{-1}. B) Nyquist plots obtained at 0.050 V using 2.0×10^{-3} M hydroquinone/benzoquinone for GCE modified with dispersions of 0.50 $mgmL^{-1}$ MWCNTs prepared in 0.25 (a), 0.50 (b), 1.00 (c) and 2.00 (d) $mgmL^{-1}$ avidin solutions. Frequency range: from 1 MHz to 0.01 Hz; potential perturbation: 10 mV; working potential: 0.050 V. C) Capacitive Nyquist diagrams obtained for 0.100 M PBS pH 7.40 at GCE/MWCNTs-avidin using GCE modified with dispersions of 0.50 $mgmL^{-1}$ MWCNTs prepared in 0.25 (a), 0.50 (b), 1.00 (c) and 2.00 (d) $mgmL^{-1}$ avidin solutions. Frequency range: from 1 MHz to 0.01 Hz; amplitude: 10 mV; working potential: 0.00 V. D) Sensitivities for hydrogen peroxide obtained from amperometric experiments at 0.700 V as a function of the avidin concentration in the dispersion used to modify GCE. Supporting electrolyte: 0.100 M PBS pH 7.40.

Fig. 2B displays Nyquist plots obtained at 0.050 V for GCE modified with dispersions of 0.50 $mgmL^{-1}$ MWCNTs prepared in 0.25 (a), 0.50 (b), 1.00 (c) and 2.00 (d) $mgmL^{-1}$ avidin solutions using 2.0×10^{-3} M hydroquinone/benzoquinone. R_{ct} increases with the increment of avidin concentration in the dispersion used to modify GCE up to 1.00 $mgmL^{-1}$, to slightly decreases thereafter. To obtain complementary information about the accessibility of MWCNTs for the charge transfer and to make a correlation with the EIS results, we also studied the system by electrochemical capacitance spectroscopy (ECS). Considering that ECS provides a purely capacitive electroanalytical signal (at lower frequencies) associated with the electronic states of CNTs [26–31], is possible to know the effect of the functionalization of MWCNTs with avidin on the electrochemical capacitance of the carbon nanostructures and on their density of electronic states. The plot of real capacitance versus applied potential displayed in Fig SI-1a indicates that the density of electronic states for MWCNTs is energetically accessible along a wide range of potentials, being maximum at 0.000V. Fig SI-1b shows that the capacitance for GCE/MWCNTs-avidin is lower than that for GCE/MWCNTs because the density of electronic states decreases when the nanostructures are modified with avidin due to the intimate contact between the carbon nanostructures and the protein. Therefore, is possible to follow the functionalization of MWCNTs with the non-conductive avidin from the decrease of the electronic states density at a given potential, being 0.000V the selected one according to the results shown in Figure SI-1a. Fig. 2C shows the plots of imaginary versus real capacitance obtained at GCEs modified with MWCNTs dispersed in 0.25 (a), 0.50 (b), 1.00 (c) and 2.00 (d) $mgmL^{-1}$ avidin solutions, for frequencies ranging from 1 MHz to 0.1 Hz with an amplitude of 10 mV. The electrochemical capacitance decreases with the increment of avidin concentration used to functionalize the MWCNTs, being minimum at 1.00 $mgmL^{-1}$, indicating that the degree of MWCNTs functionalization increases with the concentration of avidin and reaches a maximum for 1.00 $mgmL^{-1}$.

Fig. 2D shows the variation of the sensitivities for hydrogen peroxide obtained from amperometric experiments at 0.700 V as a function of the avidin concentration in the dispersion used to modify GCE. From the analysis of the results shown in this figure, is possible to get the following conclusions: i) Compared to GCE/MWCNTs, the sensitivity largely decreases for GCE/MWCNTs-avidin (0.25$mgmL^{-1}$), clearly indicating that the protein produces a blockage of the surface; ii) Compared to GCE/MWCNTs-avidin (0.25$mgmL^{-1}$), for GCE/MWCNTs-avidin prepared with increasing concentrations of avidin, the sensitivity increases with the increment of avidin up to 1.00 $mgmL^{-1}$, demonstrating that, even when the protein blocks the electrode surface, its effect on the disaggregation of the carbon nanostructures is very important and partially compensates the blocking effect; iii) Although the sensitivity increases with the amount of avidin in the dispersion due to the disaggregation of the carbon nanostructures, the sensitivity for GCE/MWCNTs-avidin never reaches the value obtained at GCE/MWCNTs. These results demonstrate the importance of the concentration of avidin solution used to non-covalenty functionalize the CNTs to obtain the best compromise between the efficiency to exfoliate the nanostructures and the negative effect of the surface blockage.

Figure SI-2 displays typical FE-SEM pictures for glassy carbon

disks modified with dispersions prepared by sonicating for 5.0 min 0.50 mgmL^{-1} of MWCNTs with 0.10 (A), 0.50 (B) and 1.00 (C) mgmL^{-1} avidin. The comparison of the different images indicates that when the glassy carbon disks are modified with dispersions containing lower amounts of avidin, there are areas with higher density of aggregates. These areas decrease when the concentration of protein used to prepare the dispersion increases, demonstrating the importance of the amount of avidin for an efficient disaggregation of the carbon nanostructures, in consonance with the voltammetric, impedimetric and amperometric results previously shown.

The aggregation fraction (χ_{agg}) is an important parameter to evaluate the efficiency of a given molecule to disaggregate the CNTs [32]. In this case, we calculate χ_{agg} by measuring the absorbance at 600 nm (inset Fig. 3) before (A_{before}) and after (A_{after}) centrifugation of MWCNTs-avidin dispersion (at 9000 rpm for 15 min) as a function of the avidin concentration, according to:

$$x_{agg} = \frac{A_{before} - A_{after}}{A_{before}}$$

Fig. 3 displays the variation of χ_{agg} with the concentration of avidin in the solution used to prepare the dispersion. χ_{agg} decreases as the concentration of avidin increases, reaching a minimum for 1.00 mgmL^{-1} avidin, indicating that the concentration of avidin that allows the disaggregation of 0.50 mgmL^{-1} MWCNTs, known as dispersion limit, is 1.00 mgmL^{-1}. The hydrodynamic radius for MWCNT-avidin decreased with the increment of the avidin concentration used to prepare the dispersions due to the disaggregation of MWCNTs bundles, reaching almost constant values for avidin concentrations higher than 1.0 mgmL^{-1} (results not shown).

In summary, the electrochemical results obtained using EIS, ECS, cyclic voltammetry and amperometry, SEM images and χ_{agg}, clearly demonstrate that there is a critical value of avidin concentration high enough to allow an efficient disaggregation of MWCNTs, but not too high to minimize the blocking effect. This optimum value was 1.0 mgmL^{-1} avidin.

3.2. Molecular recognition of GCE/MWCNTs-avidin towards b-HRP

The main goal of this work was to create a multipurpose platform for the development of different biosensors by taking advantage of the bioaffinity properties of the avidin that supports the MWCNTs through the incorporation of the corresponding biotynilated-biorecognition molecule. Therefore, is very important to know if the avidin that supports the MWCNTs presents some grade of denaturation and if it is able to recognize the biotin residues even despite the drastic conditions for the preparation of MWCNTs-avidin dispersion.

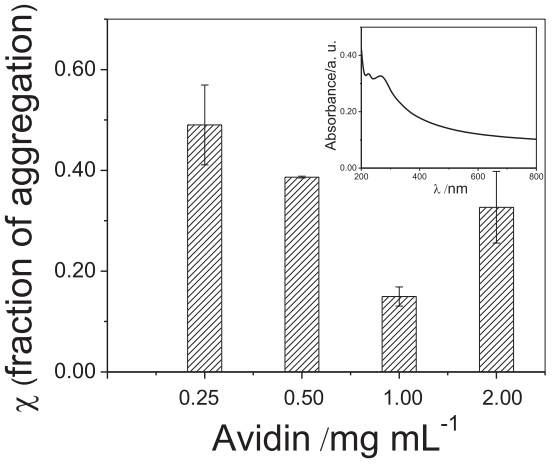

Fig. 3. Variation of χ_{agg} with the concentration of avidin in the solution used to prepare the dispersion of 0.50 mgmL^{-1} MWCNTs. Inset: UV-Vis spectra for 0.50 mgmL^{-1} MWCNTs dispersed in 1.00 mgmL^{-1} avidin.

To answer these questions, we interrogated the dispersion by different techniques. The small shifting in the wavelengths of maximum absorption of the protein observed in the UV-visible spectra (at 226 and 280 nm, Figure SI-3A) indicates that the drastic conditions for the preparation of the dispersion (sonication and ethanol/water solution) produces only a partial denaturation of avidin [33]. Figure SI-3B shows the FTIR spectra for unmodified MWCNTs (a), avidin (b) and MWCNTs-avidin (c). In the case of the spectrum corresponding to the carbon nanostructures, there is a weak band at 1648 cm^{-1} which is assigned to C=C stretching of phenyl ring vibration. The spectrum corresponding to avidin (b) presents the characteristic bands of the peptidic bonds, amide I, due to C=O stretching vibration (1654 cm^{-1}), and amide II, primarily due to the N–H bending with a contribution from C–N stretching vibrations (1538 cm^{-1}). The spectrum for MWCNTs-avidin (1.00 mgmL^{-1}) shows these two amide bands with small changes in the wavenumbers, indicating the successful attachment of the protein to the carbon nanostructures. Taking into account that amide I band is very sensitive to modifications in the secondary structure of the proteins [34,35], and that the changes in the position of this band are small, there is only a partial denaturation of the protein. Circular dichroism spectra also showed a shifting in the bands and a change of the intensity compatible with some grade of denaturation (Figure SI-3C). However, even when there is a partial denaturation of the protein, the secondary structure is preserved [36].

In this work we use b-HRP as proof-of-concept of the bioaffinity of the avidin that supports the MWCNTs towards biotin residues. We studied by SPR the immobilization of 1.00 mgmL^{-1} b-HRP (Fig. 4A, a) and HRP (Fig. 4A and b) at gold surfaces modified with MWCNT-avidin dispersion. The amount of b-HRP immobilized at the platform, calculated from the change in the plasmon resonance angle ($\Delta\theta_{SPR}$) was (2.6 ± 0.4) pmol cm^{-2}. On the contrary, when using non-biotinylated HRP instead of b-HRP, the amount of HRP at Au/MWCNT-avidin is very small (0.21 ± 0.06) pmol cm^{-2}), confirming that b-HRP is really immobilized by specific bioaffinity interaction. EIS experiments were also performed to evaluate the interaction of b-HRP and HRP with GCE/MWCNTs-avidin. Fig. 4B displays Nyquist plots obtained for 2.0×10^{-3} M hydroquinone/benzoquinone at 0.050 V at GCE/MWCNTs-avidin/b-HRP (a), GCE/MWCNTs-avidin/HRP (b) and GCE/MWCNTs-avidin (c). The considerably increase of R_{ct} after the interaction of GCE/MWCNT-avidin with b-HRP ((2.2 ± 0.3) x 10^3 Ω) compared to GCE/MWCNTs-avidin ((1.1 ± 0.3) x 10^3 Ω), and the negligible change in R_{ct} after the interaction of GCE/MWCNT-avidin with HRP ((1.1 ± 0.4) x 10^3 Ω) are additional evidences of the specific interaction between MWCNTs-avidin and b-HRP.

Fig. 4C displays cyclic voltammograms for 1.0×10^{-3} M hydroquinone obtained at GCE/MWCNT-avidin/b-HRP before (dotted line) and after (solid line) the addition of 2.0×10^{-3} M hydrogen peroxide. In the absence of hydrogen peroxide, there is a typical quasi-reversible response for hydroquinone. After the addition of hydrogen peroxide, there is a large decrease in the anodic peak current ($i_{p,a}$ = 99.8 vs 15.8 μA) and a huge increment in the cathodic one ($i_{p,c}$ = 99.1 vs 193 μA) as a consequence of the catalytic activity of b-HRP. At variance with these results, cyclic voltammograms obtained under similar conditions at GCE/MWCNTs-avidin modified with the non-biotinylated HRP (inset Fig. 4C) show negligible changes in the cathodic and anodic peak current after the addition of hydrogen peroxide ((99.8 vs 82.8 μA) for the anodic peak

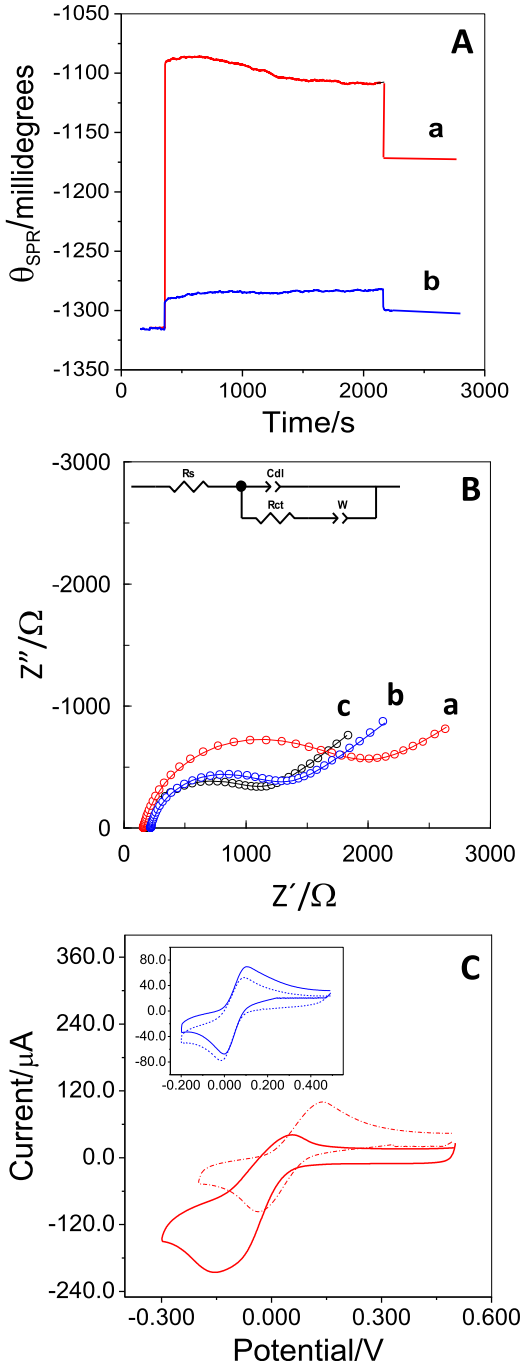

Fig. 4. A) Sensorgrams for the interaction of Au/MWCNT-avidin with b-HRP (a) and HRP (b). B)Nyquist plots obtained for 2.0×10^{-3} M hydroquinone/benzoquinone at 0.050 V at GCE/MWCNTs-avidin/b-HRP (a), GCE/MWCNTs-avidin/HRP (b) and GCE/MWCNTs-avidin (c). C)Cyclic voltammograms for 1.0×10^{-3} M hydroquinone obtained at GCE/MWCNT-avidin/b-HRP before (dotted line) and after (solid line) the addition of 2.0×10^{-3} M hydrogen peroxide for GCE/MWCNTs-avidin/b-HRP. Inset: Similar to Fig. 4C using GCE/MWCNTs-avidin/HRP.

currents and (91.5 μA vs 99.1 μA) for the cathodic peak currents in the presence and absence of hydrogen peroxide, respectively). These results clearly demonstrate that: i) the avidin that supports the CNTs can recognize biotin even after the partial denaturation produced during the preparation of the dispersion; ii) the non-specific interaction of HRP with GCE/MWCNTs-avidin is really negligible, and iii) the immobilized b-HRP can efficiently recognize hydrogen peroxide. Therefore, GCE/MWCNTs-avidin/b-HRP can be used as bioanalytical platform for the quantification of hydrogen peroxide.

Additional evidences of the successful recognition of b-HRP were also obtained by amperometry and ECS. Amperometric experiments performed at −0.100 V in the presence of 1.0×10^{-3} M hydroquinone demonstrated that the sensitivity obtained for successive additions of hydrogen peroxide with GCE/MWCNTs-avidin/b-HRP was almost five times higher than the one obtained with GCE/MWCNTs-avidin/HRP (Figure SI-4). ECS experiments performed in a 0.100 M PBS solution pH 7.40 with GCE/MWCNTs-avidin, GCE/MWCNTs-avidin/b-HRP and GCE/MWCNTs-avidin/HRP demonstrated that the capacitances for GCE/MWCNTs-avidin/HRP and GCE/MWCNTs-avidin are almost the same and clearly different than the one obtained for GCE/MWCNTs-avidin/b-HRP (Figure SI-5). Thus, SPR, EIS, cyclic voltammetry, amperometry and ECS clearly demonstrate that the avidin that supports the MWCNTs maintains its biorecognition properties making possible the successful specific immobilization of b-HRP.

The optimization of b-HRP concentration and interaction time between GCE/MWCNTs-avidin and b-HRP was performed using different techniques. Figure SI-6A displayed the variation of the SPR angle during the interaction of Au/MWCNTs-avidin prepared with different concentrations of avidin with 1.00 mgmL^{-1} b-HRP. The surface coverage of b-HRP increases with the amount of avidin present at the MWCNTs-avidin gold modified surfaces up to 1.00 mgmL^{-1} avidin (Figure SI-6B), indicating that 1.0 mgmL^{-1} avidin is also adequate to reach an efficient immobilization of b-HRP.

The optimum concentration and interaction time of b-HRP with Au/MWCNTs-avidin were selected using different techniques. EIS experiments performed with Au/MWCNTs-avidin modified with increasing concentrations of b-HRP after 15 min interaction demonstrated that R_{ct} increases with the concentration of b-HRP from 0.25 to 1.00 mgmL^{-1}, to level off thereafter (Fig. SI-7). Similar EIS experiments performed with GCE/MWCNTs-avidin modified with 1.00mgmL^{-1} b-HRP after different interaction times indicate that the optimum interaction time between Au/MWCNTs-avidin and b-HRP was 20 min (Figure SI-8A). These results were confirmed by amperometric experiments performed at −0.100 V in the presence of 1.0×10^{-3} M hydroquinone since the sensitivity for hydrogen peroxide increases with the interaction time, reaching an almost constant value between 15 and 20 min (Figure SI-8B).

3.3. Analytical performance of GCE/MWCNTs-avidin/b-HRP for hydrogen peroxide biosensing

Fig. 5A displays amperometric recordings obtained at GCE/MWCNTs-avidin/b-HRP at −0.100 V for successive additions of 1.0×10^{-6} M H_2O_2 in the presence of 1.0×10^{-5} M hydroquinone. A fast an well-defined response is observed after each addition of hydrogen peroxide. The corresponding calibration plot is shown in Fig. 5B. The linear range goes from 1.0×10^{-6} M to 1.4×10^{-5} M, with a sensitivity of $(1.37 \pm 0.04) \times 10^{5}$ μAM^{-1} ($R^2 = 0.998$), and a detection limit of 24 nM (taken as 3 x standard deviation of the blank signal/sensitivity). Table 1 compares the analytical performance of our biosensor with the most relevant biosensors for hydrogen peroxide reported in the last years based on the use of enzymes and catalytic nanomaterials. The detection limit is comparable to the one obtained using a GCE modified with porous graphene and HRP [37] and lower than those obtained with different non-enzymatic and enzymatic hydrogen peroxide sensors [18,38–44]. Seetharamaiah et al. [45] reported a biosensor with a detection limit considerably lower than the one obtained with our biosensor, although it presented a more complex scheme of preparation (using a multilayers system of polytyrosine, gold nanostructures, Ti (IV) and catalase) and worked at more negative

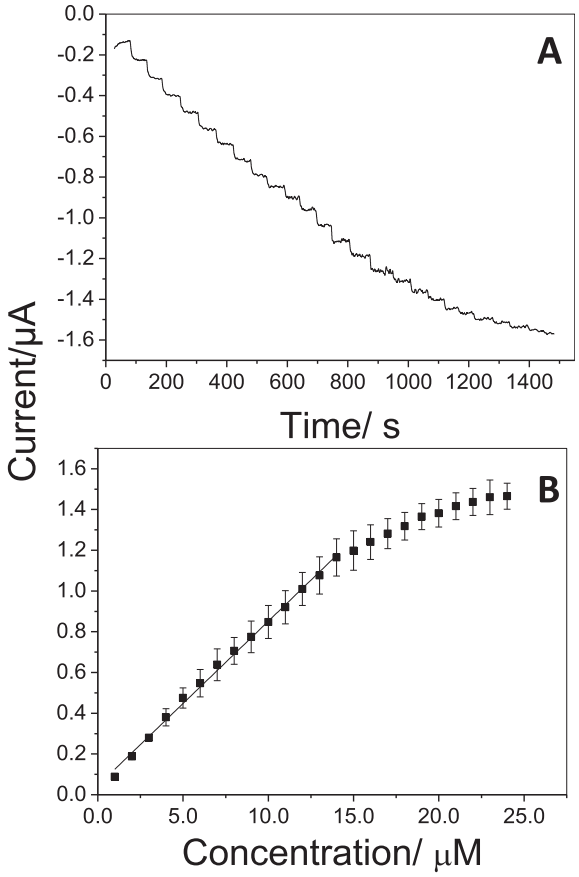

Fig. 5. A) Amperometric recordings obtained at GCE/MWCNTs-avidin/b-HRP at −0.100 V for successive additions of 1.0×10^{-6} M H_2O_2 in the presence of 1.0×10^{-5} M hydroquinone. B) Calibration plot obtained from the amperometric response at −0.100 V shown in A).

potentials (−0.400 V versus −0.100 V).

After 5 consecutive calibration plots, the sensitivity was (1.31 ± 0.04) x 10^5 μAM^{-1}, indicating a very good short-term stability. The reproducibility of GCE/MWCNTs-avidin/b-HRP using the same dispersion and 5 different electrodes was 2.9%. Amperometric experiments performed in the presence of ascorbic acid, uric acid, glucose, galactose, lactose, maltose, fructose and albumin demonstrated that the interference of these compounds is negligible (Figure SI-9).

The biosensor was challenged with different samples. The hydrogen peroxide concentration in the mouthwash "Colgate Plax Whitening" (1.5% w/w hydrogen peroxide) was (1.43 ± 0.05) % w/w, demonstrating an excellent agreement with the value reported in the product. Additionally, we determined the recovery of hydrogen peroxide in more complex samples such as human blood serum and milk, without any pre-treatment. In both cases, the samples were enriched with 25 μM hydrogen peroxide. The concentration of hydrogen peroxide obtained in human blood serum samples (Standatrol S-E-2, Wiener Lab.) diluted 1/10 with PBS was (26.3 ± 0.4) μM. The recovery percentage in milk samples diluted 1/500 with PBS was 90.8%. These successful results demonstrate the analytical usefulness of the proposed biosensor for the highly sensitive and selective quantification of hydrogen peroxide in different samples.

4. Conclusions

In summary, we demonstrated that avidin successfully disperses MWCNTs and the resulting MWCNTs-avidin platform is able to recognize biotin residues even after the drastic conditions to prepare the dispersion. The bioaffinity properties of GCE/MWCNTs-avidin and the usefulness as building-block for the development of biosensors was demonstrated using biotinylated HRP as proof-of-concept. The resulting biosensor allowed the highly sensitive quantification of hydrogen peroxide with highly competitive

Table 1
Analytical characteristics of different hydrogen peroxide electrochemical sensors.

Platform	Detection	Sensitivity	Detection Limit [μM]	Linear Range [μM]	Real sample	Ref.
PEDOT:PSS-rGO-AuNPs-HRP/ SPGEs	Amperometry E = −0.4 V	677 μA$mM^{-1}cm^{-2}$ −2	0.08	5 to 400	Tap water and bovine milk	[38]
SPE/CRGO/GCE	Amperometry E = −0.090 V	4.4 A M^{-1}	0.05	0.15–3.0	Contact lens care solutions	[39]
Nafion/Hb/FF-G/GCE	Amperometry E = −0.4 V	–	0.1	0.5–500.0	Human urine	[40]
HRP-PGN/GCE	Chronoamperometry E = −0.7 V	0.0052 μAμM^{-1}	0.0267	2.77–835	Living cells	[37]
HB/PCS/MWCNT/CPE	CV	76.43 μA$mM^{-1}cm^{-1}$	32	100–5000	–	[18]
HRP-MIL-100(Cr)-B/GCE	Amperometry E = −0.3 V	47.9 μA mM^{-1}	0.1	5–300	Living cells	[41]
Hb-PIT@Fe3O4/GCE	Amperometry E = −0.28 V	–	0.54	2–350	Rain water, milk and urine	[42]
Poly-Tyr/AuNs{1/Ti(IV)/2/AuNs/ CAT}3	Amperometry E = −0.4 V	992 μAmM^{-1} cm^{-2}	0.00098	50–19350	–	[45]
3D-KSC/PCN-333(Al)@MP-11	Amperometry E = −0.4 V	168 μA mM^{-1} cm^{-2}		0.387–1725	–	[43]
Cytc-MWCNTs/GCE	Amperometry E = −0.1 V	43 ± 1 mA M^{-1} cm^{-2}	0.15	1–160	Mouthwash and milk	[44]
b-HRP/MWCNT-avidin/GCE	Amperometry E = −0.1 V	(1.37 ± 0.04) × 10^5 μAM^{-1}	0.024	1–14	Mouthwash, milk and human blood serum	This work

Abbreviations: PEDOT: poly(3,4-ethylenedioxythiophene), PSS: poly(styrenesulfonate), rGO: reduced graphene oxide; AuNPS: gold nanoparticles; HRP: horseradish peroxidase; SPGEs: screen printed gold electrode; SPE: soybean peroxidase; CRGO: chemically reduced graphene oxide; GCE: glassy carbon electrode; HB: hemoglobin; FF-G: self-assembled nanowires of diphenylalanine and graphene nanocomposites; PGN: porous graphene; PCS: polyaniline/Multiwall Carbon Nanotubes/Starch; CPE: carbon paste electrode; MIL-100(Cr)-B: boronic acid functionalized metal-organic frameworks; PIT@Fe_3O_4: polymerized poly(indole-co-thiophene) supported Fe_3O_4; poly-Tyr: poly-tyrosine; AuNs{1/Ti(IV)/2/AuNs/CAT}3; one dimensional gold nanostructures (AuNs) and catalase (CAT) multilayer film fabricated through metal-ion coordination assembly technique using Ti (IV). PCN-333(Al)@MP: microperoxidase-11 encapsulated in metal-organic frameworks, PCN-333 (Al): stands for porous coordination network; 3DKSC: three-dimensional kenaf stem-derived porous carbon; Cytc: cytochrome *c*.

analytical characteristics.

The versatility of the proposed platform (GCE/MWCNTs-avidin) makes it extremely attractive for the development of different biosensors either enzymatic biosensors, immunosensors, genosensors, aptasensors or glycobiosensors, just by changing the biotinylated molecules used as biorecognition element attached to GCE/MWCNT-avidin.

Acknowledgements

The authors thank PIP-CONICET (PIP 2015), SECyT- UNC (2018–2021) and PICT 2016-1261 for the financial support.

Appendix A. Supplementary data

Supplementary data to this article can be found online at https://doi.org/10.1016/j.aca.2019.03.022.

References

[1] G. Maduraiveeran, M. Sasidharan, V. Ganesan, Electrochemical sensor and biosensor platforms based on advanced nanomaterials for biological and biomedical applications, Biosens. Bioelectron. 103 (2018) 113–129, https://doi.org/10.1016/j.bios.2017.12.031.

[2] S. Gupta, C.N. Murthy, C.R. Prabha, Recent advances in carbon nanotube based electrochemical biosensors, Int. J. Biol. Macromol. 108 (2018) 687–703, https://doi.org/10.1016/j.ijbiomac.2017.12.038.

[3] Z. Zhu, An overview of carbon nanotubes and graphene for biosensing applications, Nano-Micro Lett. 9 (2017) 1–24, https://doi.org/10.1007/s40820-017-0128-6.

[4] T. Feng, Y. Wang, X. Qiao, Recent advances of carbon nanotubes-based electrochemical immunosensors for the detection of protein cancer biomarkers, Electroanalysis 29 (2017) 662–675, https://doi.org/10.1002/elan.201600512.

[5] G.A. Rivas, M.C. Rodríguez, M.D. Rubianes, F.A. Gutierrez, M. Eguílaz, P.R. Dalmasso, E.N. Primo, C. Tettamanti, M.L. Ramírez, A. Montemerlo, P. Gallay, C. Parrado, Carbon nanotubes-based electrochemical (bio)sensors for biomarkers, Appl. Mater. Today 9 (2017) 566–588, https://doi.org/10.1016/j.apmt.2017.10.005.

[6] J.N. Tiwari, V. Vij, K.C. Kemp, K.S. Kim, Engineered carbon-nanomaterial-based electrochemical sensors for biomolecules, ACS Nano (2016), https://doi.org/10.1021/acsnano.5b05690.

[7] A. Setaro, Advanced carbon nanotubes functionalization, J. Phys. Condens. Matter 29 (2017), https://doi.org/10.1088/1361-665X/aa8886, 0–28.

[8] M.S. Ata, R. Poon, A.M. Syed, J. Milne, I. Zhitomirsky, New developments in non-covalent surface modification, dispersion and electrophoretic deposition of carbon nanotubes, Carbon N. Y. 130 (2018) 584–598, https://doi.org/10.1016/j.carbon.2018.01.066.

[9] D. Baskaran, J.W. Mays, M.S. Bratcher, Noncovalent and nonspecific molecular interactions of polymers with multiwalled carbon nanotubes, Chem. Mater. 17 (2005) 3389–3397, https://doi.org/10.1021/cm047866e.

[10] W. Zhao, T. Kang, L. Lu, S. Cheng, Electrochemical magnetic imprinted sensor based on MWCNTs @ CS/CTABr surfactant composites for sensitive sensing of diethylstilbestrol, J. Electroanal. Chem. 818 (2018) 181–190, https://doi.org/10.1016/j.jelechem.2018.04.036.

[11] A.S. Arribas, E. Bermejo, M. Chicharro, A. Zapardiel, G.L. Luque, N.F. Ferreyra, G.A. Rivas, Analytical applications of glassy carbon electrodes modified with multi-wall carbon nanotubes dispersed in polyethylenimine as detectors in flow systems, Anal. Chim. Acta 596 (2007) 183–194, https://doi.org/10.1016/j.aca.2007.06.014.

[12] G.L. Luque, N.F. Ferreyra, A. Granero, S. Bollo, G.A. Rivas, Electrooxidation of DNA at glassy carbon electrodes modified with multiwall carbon nanotubes dispersed in polyethylenimine, Electrochim. Acta 56 (2011) 9121–9126, https://doi.org/10.1016/j.electacta.2011.07.036.

[13] R. Savalia, S. Chatterjee, Sensitive detection of brucine an anti-metastatic drug for hepatocellular carcinoma at carbon nanotubes – nafion composite based biosensor, Biosens. Bioelectron. 98 (2017) 371–377, https://doi.org/10.1016/j.bios.2017.07.011.

[14] S. Soylemez, B. Yoon, L. Toppare, T.M. Swager, Quaternized polymer-single-walled carbon nanotube scaffolds for a chemiresistive glucose sensor, ACS Sens. 2 (2017) 1123–1127, https://doi.org/10.1021/acssensors.7b00323.

[15] Y. Jalit, M.C. Rodríguez, M.D. Rubianes, S. Bollo, G.A. Rivas, Glassy carbon electrodes modified with multiwall carbon nanotubes dispersed in polylysine, Electroanalysis 20 (2008) 1623–1631, https://doi.org/10.1002/elan.200804259.

[16] A. Gutiérrez, F. Gutierrez, M. Eguílaz, C. Parrado, G.A. Rivas, Non-covalent functionalization of multi-wall carbon nanotubes with polyarginine: characterization and analytical applications for uric acid quantification, Electroanalysis 30 (2018) 1416–1424, https://doi.org/10.1002/elan.201800034.

[17] P.R. Dalmasso, M.L. Pedano, G.A. Rivas, Supramolecular architecture based on the self-assembling of multiwall carbon nanotubes dispersed in polyhistidine and glucose oxidase: characterization and analytical applications for glucose biosensing, Biosens. Bioelectron. 39 (2013) 76–81, https://doi.org/10.1016/j.bios.2012.06.041.

[18] V. Gautam, K.P. Singh, V.L. Yadav, Polyaniline/multiwall carbon nanotubes/starch nanocomposite material and hemoglobin modified carbon paste electrode for hydrogen peroxide and glucose biosensing, Int. J. Biol. Macromol. 111 (2018) 1124–1132, https://doi.org/10.1016/j.ijbiomac.2018.01.094.

[19] F. Gutierrez, M.D. Rubianes, G.A. Rivas, Dispersion of multi-wall carbon nanotubes in glucose oxidase: characterization and analytical applications for glucose biosensing, Sensor. Actuator. B Chem. 161 (2012) 191–197, https://doi.org/10.1016/j.snb.2011.10.010.

[20] M. Eguílaz, R. Villalonga, J.M. Pingarrón, N.F. Ferreyra, G.A. Rivas, Functionalization of bamboo-like carbon nanotubes with 3-mercaptophenylboronic acid-modified gold nanoparticles for the development of a hybrid glucose enzyme electrochemical biosensor, Sensor. Actuator. B Chem. 216 (2015) 629–637, https://doi.org/10.1016/j.snb.2015.03.112.

[21] M. Eguílaz, C.J. Venegas, A. Gutiérrez, G.A. Rivas, S. Bollo, Carbon nanotubes non-covalently functionalized with cytochrome c: a new bioanalytical platform for building bienzymatic biosensors, Microchem. J. 128 (2016) 161–165, https://doi.org/10.1016/j.microc.2016.04.018.

[22] E.N. Primo, P. Cañete-Rosales, S. Bollo, M.D. Rubianes, G. a. Rivas, Dispersion of bamboo type multi-wall carbon nanotubes in calf-thymus double stranded DNA, Colloids Surfaces B Biointerfaces 108 (2013) 329–336, https://doi.org/10.1016/j.colsurfb.2013.02.028.

[23] E.N. Primo, M.B. Oviedo, C.G. Sánchez, M.D. Rubianes, G. a. Rivas, Bioelectrochemical sensing of promethazine with bamboo-type multiwalled carbon nanotubes dispersed in calf-thymus double stranded DNA, Bioelectrochemistry 99 (2014) 8–16, https://doi.org/10.1016/j.bioelechem.2014.05.002.

[24] R.L. McCreery, Advanced carbon electrode materials for molecular electrochemistry, Chem. Rev. 108 (2008) 2646–2687, https://doi.org/10.1021/cr068076m.

[25] E.N. Primo, F.A. Gutierrez, G.L. Luque, P.R. Dalmasso, A. Gasnier, Y. Jalit, M. Moreno, M.V. Bracamonte, M.E. Rubio, M.L. Pedano, M.C. Rodríguez, N.F. Ferreyra, M.D. Rubianes, S. Bollo, G.A. Rivas, Comparative study of the electrochemical behavior and analytical applications of (bio)sensing platforms based on the use of multi-walled carbon nanotubes dispersed in different polymers, Anal. Chim. Acta 805 (2013) 19–35, https://doi.org/10.1016/j.aca.2013.10.039.

[26] P.R. Bueno, G.T. Feliciano, J.J. Davis, Capacitance spectroscopy and density functional theory, Phys. Chem. Chem. Phys. 17 (2015) 9375–9382, https://doi.org/10.1039/c4cp06015f.

[27] D.A. Miranda, P.R. Bueno, Density functional theory and an experimentally-designed energy functional of electron density, Phys. Chem. Chem. Phys. 18 (2016) 25984–25992, https://doi.org/10.1039/c6cp01659f.

[28] P.R. Bueno, F. Fabregat-Santiago, J.J. Davis, Elucidating capacitance and resistance terms in confined electroactive molecular layers, Anal. Chem. 85 (2013) 411–417, https://doi.org/10.1021/ac303018d.

[29] P.R. Bueno, J.J. Davis, Elucidating redox-level dispersion and local dielectric effects within electroactive molecular films, Anal. Chem. 86 (2014) 1997–2004, https://doi.org/10.1021/ac4031708.

[30] P.R. Bueno, G. Mizzon, J.J. Davis, Capacitance spectroscopy: a versatile approach to resolving the redox density of states and kinetics in redox-active self-assembled monolayers, J. Phys. Chem. B 116 (2012) 8822–8829, https://doi.org/10.1021/jp303700f.

[31] P.R. Bueno, J.J. Davis, Measuring quantum capacitance in energetically addressable molecular layers, Anal. Chem. 86 (2014) 1337–1341, https://doi.org/10.1021/ac403135b.

[32] Q. Cheng, E. Gregan, H. Byrne, Ultrasound-assisted SWNTs Dispersion : effects of sonication parameters and solvent properties ultrasound-assisted SWNTs dispersion : effects of sonication parameters and solvent properties, J. Phys. Chem. C 114 (2010) 8821–8827.

[33] N.M. Green, M.D. Melamed, Optical rotatory dispersion, circular dichroism and far-ultraviolet spectra of avidin and streptavidin, Biochem. J. 100 (1966) 614–621, https://doi.org/10.1042/bj1000614.

[34] M. Hereć, M. Gagoś, M. Kulma, K. Kwiatkowska, A. Sobota, W.I. Gruszecki, Secondary structure and orientation of the pore-forming toxin lysenin in a sphingomyelin-containing membrane, Biochim. Biophys. Acta Biomembr. 1778 (2008) 872–879, https://doi.org/10.1016/j.bbamem.2007.12.004.

[35] G. Palestino, R. Legros, V. Agarwal, E. Pérez, C. Gergely, Functionalization of nanostructured porous silicon microcavities for glucose oxidase detection, Sensor. Actuator. B Chem. 135 (2008) 27–34, https://doi.org/10.1016/j.snb.2008.07.013.

[36] F. Wang, P.L. Polavarapu, Temperature influence on the secondary structure of avidin and avidin-biotin complex: a vibrational circular dichroism study, J. Phys. Chem. B 105 (2001) 7857–7864, https://doi.org/10.1021/jp0104177.

[37] Y. Liu, X. Liu, Z. Guo, Z. Hu, Z. Xue, X. Lu, Horseradish peroxidase supported on porous graphene as a novel sensing platform for detection of hydrogen peroxide in living cells sensitively, Biosens. Bioelectron. 87 (2017) 101–107, https://doi.org/10.1016/j.bios.2016.08.015.

[38] L.A. Mercante, M.H.M. Facure, R.C. Sanfelice, F.L. Migliorini, L.H.C. Mattoso, D.S. Correa, One-pot preparation of PEDOT: PSS-reduced graphene decorated with Au nanoparticles for enzymatic electrochemical sensing of H2O2, Appl. Surf. Sci. 407 (2017) 162–170, https://doi.org/10.1016/j.apsusc.2017.02.156.

[39] C.H. Díaz Nieto, A.M. Granero, J.C. Lopez, G.D. Pierini, G.J. Levin, H. Fernández, M.A. Zon, Development of a third generation biosensor to determine hydrogen peroxide based on a composite of soybean peroxidase/chemically reduced graphene oxide deposited on glassy carbon electrodes, Sensor. Actuator. B Chem. 263 (2018) 377–386, https://doi.org/10.1016/j.snb.2018.02.094.

[40] Y. Wu, F. Wang, K. Lu, M. Lv, Y. Zhao, Self-assembled dipeptide-graphene nanostructures onto an electrode surface for highly sensitive amperometric hydrogen peroxide biosensors, Sensor. Actuator. B Chem. 244 (2017) 1022–1030, https://doi.org/10.1016/j.snb.2017.01.048.

[41] H. Dai, W. Lü, X. Zuo, Q. Zhu, C. Pan, X. Niu, J. Liu, H.L. Chen, X. Chen, A novel biosensor based on boronic acid functionalized metal-organic frameworks for the determination of hydrogen peroxide released from living cells, Biosens. Bioelectron. 95 (2017) 131–137, https://doi.org/10.1016/j.bios.2017.04.021.

[42] M. Baghayeri, M. Rouhi, M.M. Lakouraj, M. Amiri-Aref, Bioelectrocatalysis of hydrogen peroxide based on immobilized hemoglobin onto glassy carbon electrode modified with magnetic poly(indole-co-thiophene) nanocomposite, J. Electroanal. Chem. 784 (2017) 69–76, https://doi.org/10.1016/j.jelechem.2016.12.006.

[43] C. Gong, Y. Shen, J. Chen, Y. Song, S. Chen, Y. Song, L. Wang, Sensors and Actuators B : Chemical Microperoxidase-11 @ PCN-333 (Al)/Three-Dimensional Macroporous Carbon Electrode for Sensing Hydrogen Peroxide, vol 239, 2017, pp. 890–897.

[44] M. Eguílaz, A. Gutiérrez, G. Rivas, Non-covalent functionalization of multiwalled carbon nanotubes with cytochrome c: enhanced direct electron transfer and analytical applications, Sensor. Actuator. B Chem. 225 (2016) 74–80, https://doi.org/10.1016/j.snb.2015.11.011.

[45] N. Seetharamaiah, N. Seetharamaiah, N. Pathappa, J.S. Melo, S.S. Gurukar, Metal-ion co-ordination assembly based multilayer of one dimensional gold nanostructures and catalase as electrochemical sensor for the analysis of hydrogen peroxide, Sensor. Actuator. B Chem. 245 (2017) 726–740, https://doi.org/10.1016/j.snb.2017.02.003.